Ab initio study of structural, electronic and optical properties of Ca 1− x Sr x S compounds

ARTICLE *in* PHYSICA B CONDENSED MATTER · NOVEMBER 2009

Impact Factor: 1.32 · DOI: 10.1016/j.physb.2009.07.147

Physica B 404 (2009) 3964–3972

Contents lists available at ScienceDirect

Physica B

journal homepage: www.elsevier.com/locate/physb

Ab initio study of structural, electronic and optical properties of $Ca_{1-x}Sr_xS$ compounds

A. Shaukat [a,*], Y. Saeed [a], S. Nazir [b], N. Ikram [b], M. Tanveer [b,1]

[a] Department of Physics, GC University, 38000 Faisalabad, Pakistan
[b] Centre for Solid State Physics, University of the Punjab, 54590 Lahore, Pakistan

ARTICLE INFO

Article history:
Received 11 April 2009
Received in revised form
7 July 2009
Accepted 9 July 2009

PACS:
71.15.Mb
74.25.Gz
74.25.Jb

Keywords:
CaSrS alloys
Density functional theory
LDA
GGA
Electronic structure
Optical properties

ABSTRACT

Full-potential linearized augmented plane wave method (FP-LAPW) within density functional theory has been used to calculate structural, electronic and optical properties of $Ca_{1-x}Sr_xS$, an alkali earth chalcogenide, with varying compositional parameter x in the range $0<x<1$. Whereas the structural properties are discussed in terms of charge transfer between the two cations, calculated electronic band structure and density of states have been analyzed in terms of contribution from the S p, Ca d and Sr d states. Furthermore, we have calculated some optical properties such as real and imaginary parts of dielectric constant, $\varepsilon(\omega)$, and the calculated results have been discussed in comparison with the existing experimental data and other theoretical calculations.

1. Introduction

Alkaline-earth chalcogenides belonging to the binary group II^A–VI have recently attracted great attention of researchers because of their potential use as thermionic, photo-luminescent, phosphorescent, cathodoluminescent, magneto-optic and other opto-electronic materials [1–3]. CaS and SrS, two alkaline earth sulfides, members of the same group have proven to be excellent phosphor host materials and, since recently, are considered to be of great use in the display and opto-electronic devices [4,5]. Experimental investigations of the Te-doped solid solutions of these sulfides, $Ca_{1-x}Sr_xS$, were undertaken by Kato et al. [6] indicating that the band-gap dependence on the compositional parameter x could be utilized for tuning the photoluminescent emission spectra. Later, Brightwell et al. [7] studied composition effects on the photoluminescence properties of the undoped $Ca_xSr_{1-x}S$ material. Nanocrystallites of $Sr_{1-x}Ca_xS$ were synthesized and their luminescence properties were reported by Wang et al. [8] in the recent past.

Keeping in view the importance of these solid solutions in a variety of technological applications, we have, in this paper, studied the structural, electronic and optical properties by performing *ab initio* calculations, based on the full-potential linearized augmented plane wave method (FP-LAPW) within density functional theory as implemented in the WIEN2K code [9]. In the next section, we briefly describe the calculation procedure and give the computational details. In Section 3, we report and discuss our results for structural, electronic and optical properties of the ordered $Ca_{1-x}Sr_xS$ alloys. Finally, conclusions of the present study will be given in Section 4.

2. Computational methods

In order to study structural and electronic properties of the ordered $Ca_{1-x}Sr_xS$ alloys, we have performed self-consistent calculations using the full-potential linearized augmented plane wave method (FP-LAPW) approach based on the density functional theory, where we have used three different approximations for the calculation of exchange-correlation energy functional, namely, the standard local density approximation (LDA), the well-known generalized gradient approximation (GGA) of Perdew, Burke and Ernzerhof (PBE) [10] and the recently proposed GGA

* Corresponding author. Tel.: +92 41 920 1372; fax: +92 41 920 0671.
E-mail address: schaukat@gmail.com (A. Shaukat).
[1] Present address: Institut für Theoretische Physik, Universität Kassel, 34132 Kassel, Germany.

0921-4526/$ - see front matter © 2009 Elsevier B.V. All rights reserved.
doi:10.1016/j.physb.2009.07.147

Table 1
Calculated lattice parameter a, bulk modulus B_0, its pressure derivative and B_0' for $Ca_{1-x}Sr_xS$ alloys at equilibrium volume compared to experiment and other theoretical calculations.

$Ca_{1-x}Sr_xS$ $(0 \le x \le 1)$	Present work			Experimental works	Other theoretical works
	LDA	GGA	GGA(WC)		
CaS (B1)					
a (Å)	5.57	5.72	5.65	5.68[a], 5.69[b]	5.645[b], 5.59[b], 5.64[c]
B_0 (GPa)	68.36	56.6	61.70	64[a], 56.3[b]	62.3[b], 67.8[b], 67.4[c]
B_0'	4.16	4.12	4.12	4.2[a],4.6[b]	4.0[b], 4.15[b], 4.4[c]
$Ca_{0.75}Sr_{0.25}S$					
a (Å)	5.66	5.815	5.736		
B_0 (GPa)	65.63	54.815	59.34		
B_0'	4.35	4.26	4.31		
$Ca_{0.50}Sr_{0.50}S$					
a (Å)	5.757	5.903	5.82		
c (Å)	4.07	4.174	4.11		
B_0 (GPa)	62.91	52.413	57.41		
B_0'	4.11	4.29	4.39		
$Ca_{0.25}Sr_{0.75}S$					
a (Å)	5.83	5.98	5.898		
B_0 (GPa)	60.26	48.94	55.50		
B_0'	4.17	4.33	4.76		
SrS (B1)					
a (Å)	5.906	6.064	5.972	6.024[d]	6.076[e], 5.77[f], 6.03[e]
B_0 (GPa)	58.70	47.94	53.11	53.9[g]	47[e], 62[f], 48.24[e]
B_0'	4.34	4.34	4.47		4.19[e]

[a] Ref. [13].
[b] Ref. [14].
[c] Ref. [15].
[d] Ref. [16].
[e] Ref. [17].
[f] Ref. [21].
[g] Ref. [22].

due to Wu and Cohen (WC) [11]. For calculating optical properties, only the PBE scheme has been applied. In the FP-LAPW method, the wave function, charge density and potential are expanded by spherical harmonic functions inside non-overlapping spheres surrounding the atomic sites (muffin-tin spheres) and by a plane wave basis set in the remaining space of the unit cell (interstitial region). Muffin-tin (MT) model for the crystal potential is assumed and the muffin-tin radius R_{MT} for all the three atoms Ca, Sr and S is taken to be 2.5 a.u. Kohn–Sham wave functions are expanded in terms of spherical harmonics inside the non-overlapping MT spheres surrounding the atomic sites and the plane wave expansion is used in the interstitial region. Within the MT spheres, the l-expansion of the non-spherical potential is carried out up to $l_{MAX} = 10$ while the charge density is Fourier-expanded up to $G_{MAX} = 14$. In order to achieve energy eigenvalues convergence, the wave functions in the interstitial region are expanded in terms of plane waves with a cut-off of $K_{MAX} = 8/R_{MT}$. A mesh of 72 special **k**-points for CaS, SrS and 35 special **k**-points in $Ca_{1-x}Sr_xS$ are taken in the irreducible wedge of the Brillouin zone (IBZ). The frequency-dependent optical properties are calculated using 560 **k**-points in the IBZ. Both the R_{MT} and the number of **k**-points are varied to ensure total energy convergence within an accuracy of 10^{-6} Ry.

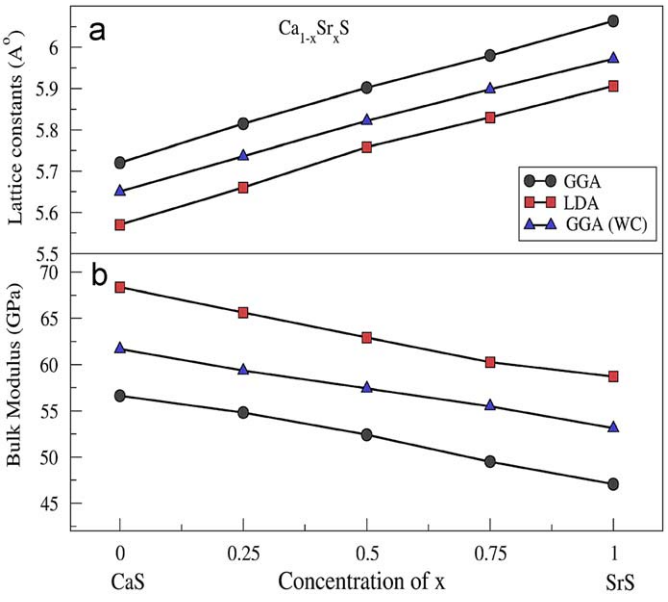

Fig. 1. Variation of (a) lattice constant and (b) bulk modulus as a function of the concentration x for $Ca_{1-x}Sr_xS$.

3. Results and discussion

3.1. Structural properties

As mentioned earlier, we have calculated the structural properties of $Ca_{1-x}Sr_xS$ compounds using all the three approximations LDA, PBE and WC with the compositional parameter x having the values 0.0, 0.25, 0.50, 0.75 and 1.0. The total energy for each composition is minimized with respect to volume using Murnaghan equation of state [12] and the results calculated for the lattice constants, bulk modulus B_0 and derivative of bulk modulus B_0' have been listed in Table 1. Our results calculated by

using WC approximation as regards the end compounds, CaS and SrS, are in good agreement with the experimental values as well as with other theoretical estimates [13–17]. On the other hand, LDA and GGA (PBE) underestimate and overestimate the values of the equilibrium lattice constants, respectively. This is in accordance with the earlier studies on solids [11,18], in which WC clearly shows significant improvement over LDA and PBE for the structural parameters and the bulk modulus. The calculated structural parameters of the solid solutions have also been summarized in Table 1, whereas Fig. 1 shows that the variation in lattice constant and the bulk modulus with the composition x obey Vegard's law [19].

Furthermore, it is noticed that the structure of the $Ca_{1-x}Sr_xS$ alloy system, undergoes a phase change from cubic-type structure (space group F_{m3m}) for the end compounds CaS ($x=0$) and SrS ($x=1$) to another cubic-type (space group $P_{m\text{-}3m}$) for the compositions $x=0.25$ and 0.75; whereas it changes to tetragonal structure (space group $P_{4/mmm}$) for $x=0.50$ as shown in Fig. 2. This structural change from cubic to tetragonal for composition $x=0.50$ may be explained in terms of charge transfer between cations and anions that also changes the nature of bond from covalent to ionic for $Ca_{0.50}Sr_{0.50}S$. This feature can be clearly observed in Fig. 3, which shows the charge density maps for the solid solution and the end compounds. These total valence charge density distribution maps, which have been calculated for all $x=0.0$, 0.25, 0.50, 0.75 and 1.0 in the $\langle 1\,0\,0\rangle$ plane containing different atoms, show ionic character of the CaS compound and $Ca_{0.50}Sr_{0.50}S$ alloy, while the presence of bonding charge is evident in case of SrS, and the $Ca_{0.25}Sr_{0.75}S$ and $Ca_{0.75}Sr_{0.25}S$ alloys. It appears that the charge transfer from the cations, Ca and Sr, towards more electronegative S (anion) may be responsible for the structural change in case of $Ca_{0.50}Sr_{0.50}S$; that is, the charge depletion towards S may have changed the structure of the alloy from cubic to tetragonal. Obviously, this change of phase

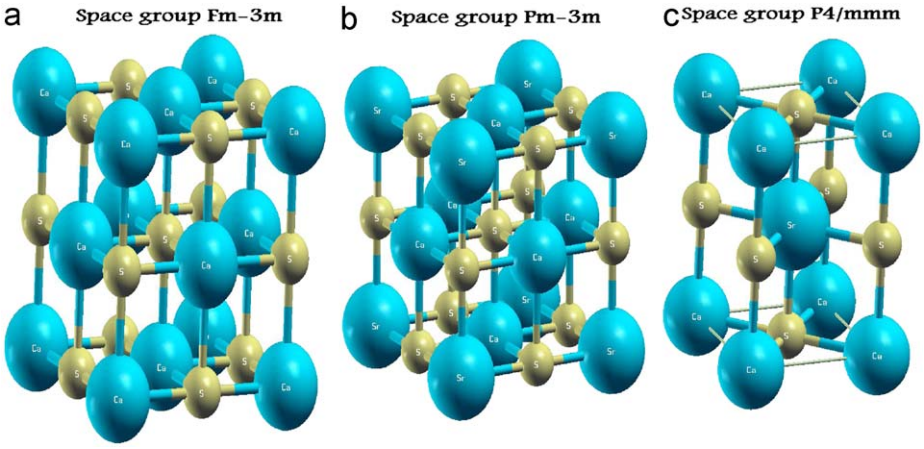

Fig. 2. Crystal structure: (a) CaS, (b) $Ca_{0.75}Sr_{0.25}S$ and (c) $Ca_{0.50}Sr_{0.50}S$ alloys.

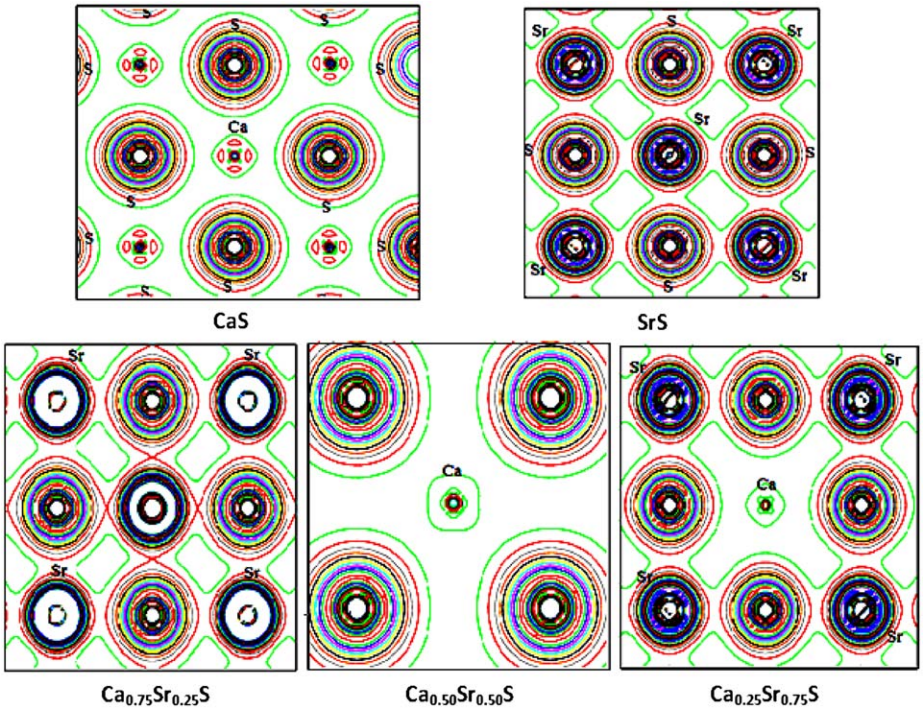

Fig. 3. Contour plots of the valence charge distribution of $Ca_{1-x}Sr_xS$ in the $\langle 1\,0\,0\rangle$ from $x=0$ to 1.

corresponding to different values of the compositional parameter x for the $Ca_{1-x}Sr_xS$ alloy system has a predictive character, which one would expect from the DFT calculations, and is subject to the experimental verification.

3.2. Electronic properties

Knowledge of the energy band structures in semiconductors provides valuable information as regards their potential utility in fabricating the electronic devices. As alkaline-earth chalcogenides are promising materials for their application in solid-state devices, accurate knowledge of the band structures of the $Ca_{1-x}Sr_xS$ alloys becomes essential. Calculated band structures of CaS, SrS and $Ca_{1-x}Sr_xS$ for different x-values, using the PBE GGA scheme, have been displayed in Fig. 4. Table 2, however, presents our calculated energy band gaps values, $E_g(\Gamma-\Gamma)$ and $E_g(\Gamma-X)$, using all the three (LDA, PBE, WC) schemes, along with the experimental and other calculated results [20–25]. As one can see here, the experimental value of the lowest *indirect* band gap, $E_g(\Gamma-X)$, for CaS is 4.434 eV, while that of the *direct* band gap at the point Γ, $E_g(\Gamma-\Gamma)$, is 5.80 eV. Calculated values of these band gaps are, however, 2.15 and 4.25 eV, respectively. For the other end compound, SrS, the experimental values for $E_g(\Gamma-X)$ and $E_g(\Gamma-\Gamma)$ are 4.32 and 5.387 eV, respectively, whereas the calculated values for these band gaps are 2.15 and 3.8 eV, respectively. The large difference in the calculated values of the band gaps as compared to the experimental values can be explained by the fact that, in the electronic band structure calculations within DFT, both LDA and GGA underestimate the energy band gap in semiconductors, and it can be demonstrated that within these approximations, the self-interaction error and the absence of

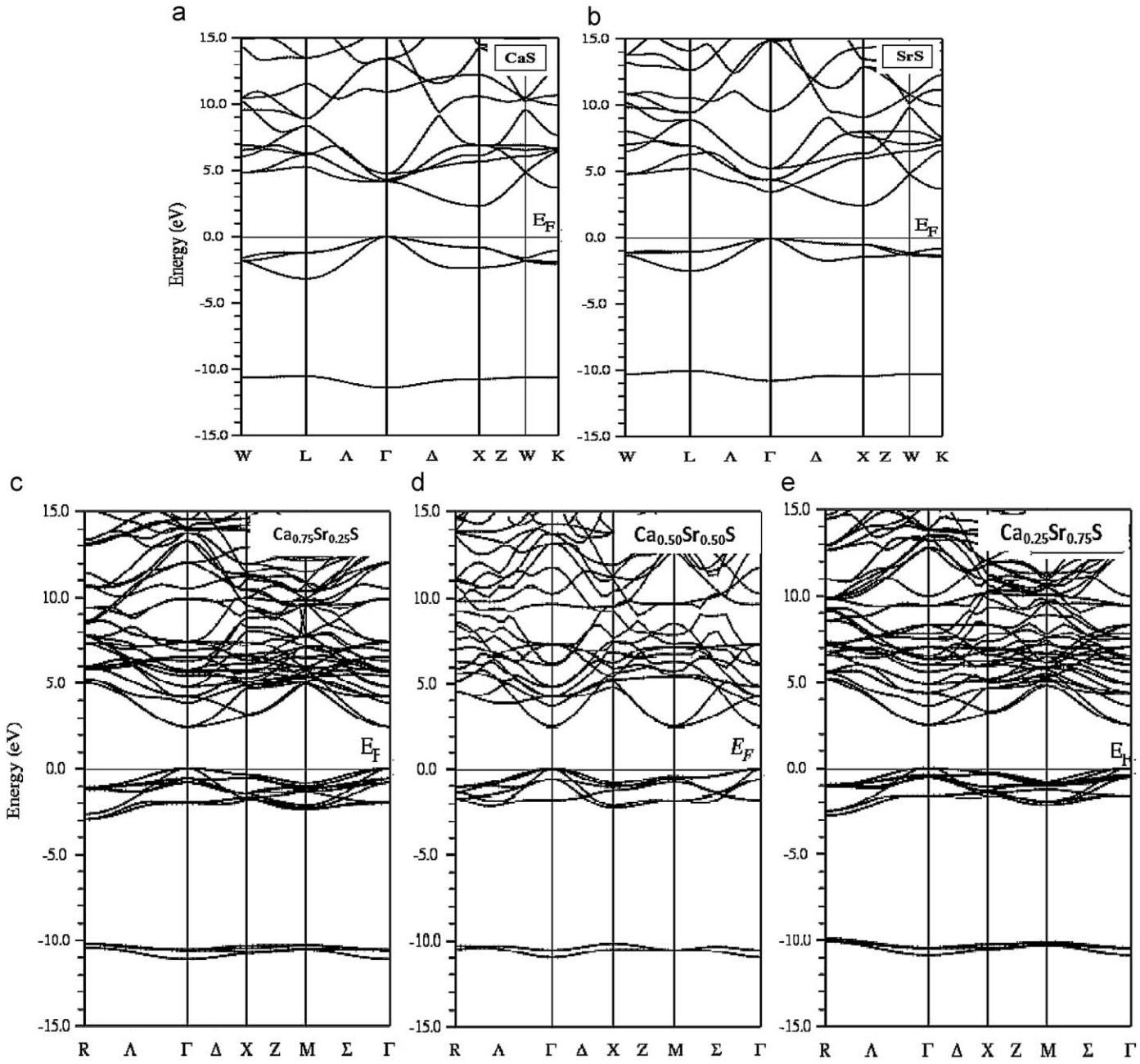

Fig. 4. Band structures of (a) CaS (b) SrS (c) $Ca_{0.75}Sr_{0.25}S$ (d) $Ca_{0.50}Sr_{0.50}S$ (e) $Ca_{0.25}Sr_{0.75}S$ along high symmetry directions in the Brillouin zone.

derivative discontinuity in the exchange-correlation potential cause a significant underestimation (up to 50%) of the band gap [26,27].

From Fig. 4, which shows the calculated band structures of $Ca_{1-x}Sr_xS$ for different compositions x (using PBE approximation), one can clearly see the nature of the band gap of these compounds. Whereas the fundamental band gap for both end compounds, CaS and SrS, is *indirect*, $E_g(\Gamma-X)$, in agreement with the experimental studies [28], it turns out to be *direct*, $E_g(\Gamma-\Gamma)$, for all the other $Ca_{0.25}Sr_{0.75}S$, $Ca_{0.50}Sr_{0.50}S$ and $Ca_{0.75}Sr_{0.25}S$ alloys.

Table 2
Calculated band gaps, $E_g(\Gamma-\Gamma)$ and $E_g(\Gamma-X)$, for $Ca_{1-x}Sr_xS$ alloy (in eV).

	LDA	GGA (PBE)	GGA (WC)	Experimental work	Theoretical work
CaS					
$E_g(\Gamma-\Gamma)$	3.9	4.25	4.2	5.80[a]	4.47[b], 7.6[c]
$E_g(\Gamma-X)$	1.9	2.15	2.1	4.434[a]	2.398[d], 3.2[e]
$Ca_{0.75}Sr_{0.25}S$					
$E_g(\Gamma-\Gamma)$	2.45	2.5	2.4		
$Ca_{0.50}Sr_{0.50}S$					
$E_g(\Gamma-\Gamma)$	2.2	2.4	2.3		
$Ca_{0.25}Sr_{0.75}S$					
$E_g(\Gamma-\Gamma)$	2.1	2.4	2.2		
SrS					
$E_g(\Gamma-\Gamma)$	3.65	3.8	3.6	5.387[a]	3.51[f]
$E_g(\Gamma-X)$	2.1	2.15	2.3	4.32[a]	2.3[d]

[a] Ref. [20].
[b] Ref. [21].
[c] Ref. [24].
[d] Ref. [15].
[e] Ref. [23].

The reason for the appearance of an indirect band gap in CaS, for example, is the lowering of the X-state (X_3 point) of the conduction band relative to its Γ_1-state, which is apparently due to the strong hybridization of the Ca 4s or 3d states with the S 3s or 3p states. Consequently, one would expect significant charge transfer to the Ca 3d states, as a result of which a lowering of X_3-state of the Ca 3d states takes place [29]. The maximum of the valence band is defined by the S 3p states and lies at the Γ_{15}-point. For CaS, therefore, the lower energy transition is expected to be the indirect transition $\Gamma_{15}-X_3$. In case of SrS, the valence bands have a character of 3p-orbitals of the S ion with the top at the Γ-point, whereas the conduction bands are composed of 5s and 4d-orbitals of Sr ion. The d-like conduction bands further split off at Γ-point and give rise to another conduction band minimum at the X-point (X_3), giving rise to the indirect band gap. Mixing of the two compounds, CaS and SrS, however, results in change of the fundamental band gap in the alloys, i.e., from indirect to the direct type.

Furthermore, Fig. 4 clearly depicts the similarity in the band structures of the two alloys, namely, $Ca_{0.25}Sr_{0.75}S$ and $Ca_{0.75}Sr_{0.25}S$, while for $Ca_{0.50}Sr_{0.50}S$ the features of the band structure are distinctly different. This is not something unexpected, keeping in view the structural symmetry of these compounds; $Ca_{0.25}Sr_{0.75}S$ and $Ca_{0.75}Sr_{0.25}S$ belong to the same space group, cubic $P_{m\text{-}3m}$, while $Ca_{0.50}Sr_{0.50}S$ has got a tetragonal structure belonging to the space group $P_{4/mmm}$.

Variation of band gap $E_g(\Gamma-\Gamma)$ with concentration x in $Ca_{1-x}Sr_xS$ alloys has been studied by using the following quadratic equations:

$$E_g(\Gamma-\Gamma) = 4.184 - 7.714x + 7.314x^2 \quad (1)$$

$$E_g(\Gamma-\Gamma) = 4.225 - 8.8x + 8.4x^2 \quad (2)$$

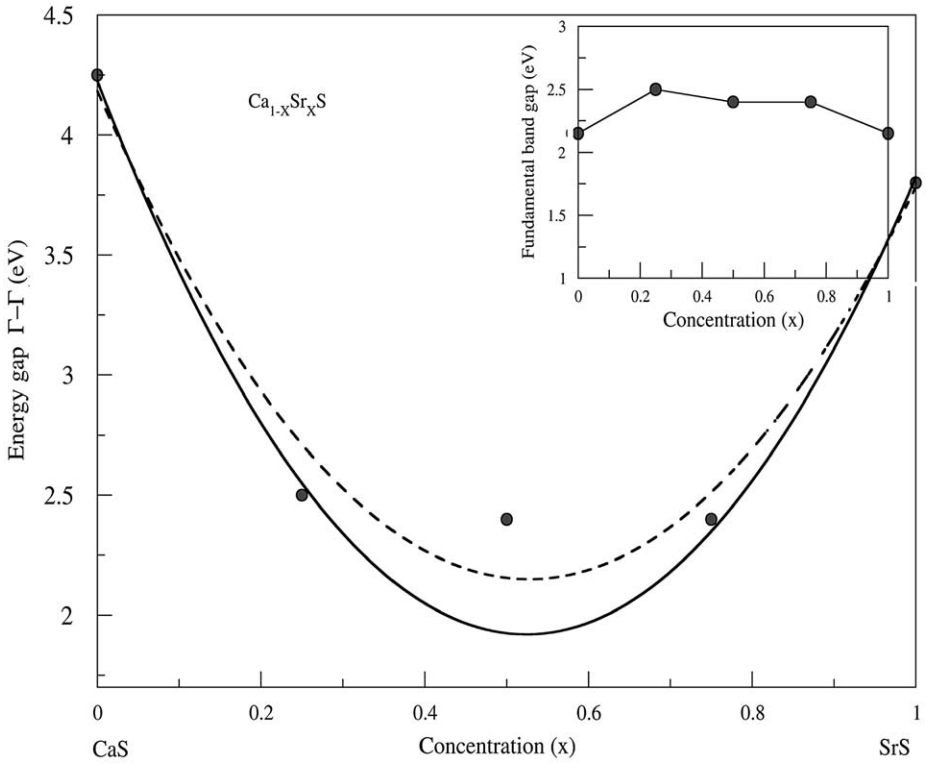

Fig. 5. The energy band gap $E_g(\Gamma-\Gamma)$ of CaS (4.25 eV) and SrS (3.8 eV) and their alloys with different concentration x. Inset shows the variation of the fundamental band gap with x.

[f] Ref. [22].

We must, however, remark that, contrary to the band gap values of the alloys, the values of the $E_g(\Gamma-\Gamma)$ of the two end compounds, CaS and SrS, taken in the above equations, are not the *lowest* (fundamental) band gap values. Here, Eq. (1) gives the best fit for all concentrations $0 \le x \le 1$ in Fig. 5, while Eq. (2) has been tried for all concentrations except for $x = 0.50$, keeping in view the structural difference in this case. The large difference in the band gaps of the alloys and the end compounds is usually attributed to charge transfer, reflected in terms of the electronegativity difference of the mixing cations or anions, volume deformation arising from the changes of their individual equilibrium lattice constants to the alloy value, and structural relaxation due to change from the unrelaxed to the relaxed alloy [30]. In the inset of Fig. 5, we have also shown the variation of the fundamental band gap of the $Ca_{1-x}Sr_xS$ alloys, which shows only a slight change in the values of the band gaps of the alloys as compared to their binaries; the nature of the band gap for the alloys is, however, different from that of the initial compounds.

Partial density of states curves (PDOS) for $Ca_{0.25}Sr_{0.75}S$, $Ca_{0.50}Sr_{0.50}S$ and $Ca_{0.75}Sr_{0.25}S$ have been displayed in Fig. 6 in order to analyze contribution from different states of Ca, Sr and S atoms. As we can see, the first structure in the lower-lying energy side of the DOS consists of a narrow peak centered at around −10.61, −10.38 and −10.30 for these concentrations of x, while the individual peaks are due to Ca 3p, Sr 4p and S 3s states. The second structure below the Fermi level is due to the chalcogene S 3p states with small contribution from Ca 4s and Sr 5s states. Above the Fermi level we see a broad structure with its features extending up to 15 eV. Whereas its broad peak is found to have its centre at 6 eV for the end compounds CaS and SrS, it is around 7 eV for $Ca_{1-x}Sr_xS$ solid solutions. Furthermore, the PDOS for CaS, Fig. 6a, can be divided into four regions. In the first region (−10.6 to −9.6 eV) a sharp structure around −10.6 eV is visible, which is due to S 3s and Ca 3p states. When Sr is added, Sr 4p states also appear at the same position. The second region (−9.6 to 0.0 eV), i.e. the top of the valence band is mainly due to S 3p, Ca 4s and Sr 5s states. The third region (from 2.5 to 8 eV), i.e. bottom of the conduction band, is composed of Ca 3d states. When Sr is added, its 4d states also come in the same region. The fourth region (from 8 eV onwards) is dominated by Sr 4p state. Our calculations show that replacing Ca by Sr causes the bandwidth of the valence band to decease slightly, and new structures become visible in the third and the fourth regions which are attributed to Sr 5s and 4p states.

3.3. Optical properties

In this section, we present our calculations for the real and imaginary parts of the dielectric constant, compare the results with the available data for CaS [20] and for SrS [17], and discuss the changes in their structure for the solid solution $Ca_{1-x}Sr_xS$. Following Khan et al. [31], the calculated imaginary part, $\varepsilon_2(\omega)$, of the dielectric constant for the end compounds and their solid solution for various values of the compositional parameter x is shown in Fig. 7(a). The detailed structure of these curves can approximately be separated in three parts according to the energy range; namely, from 0 to 10 eV, 10 to 20 eV and from 20 to 30 eV. The first critical point in the curve, which is attributed to the threshold for the direct optical transition between the valence-band maximum and the conduction-band minimum, occurs around 3.5 eV (for CaS) and shifts slightly towards a lower value as we increase the Sr component. Finally, for SrS, the threshold value reduces to around 2.5 eV, whereas the maximum of the first strong peak shifts towards a higher value, i.e., from 6.17 eV (CaS) to 6.78 eV (SrS). The first peak appears to be occurring from the electronic transition between Ca 4d, Sr 4d and S 3p states for CaS and SrS, respectively. Transitions between the Ca 4d, Sr 4d and S 3s states may lead to the occurrence of smaller peaks in the energy range 10–20 eV, whereas the prominent peaks appearing in the third energy range (20–30 eV) seem to be the result of transition between the Ca 4s, Sr 5s S 3p and Ca 3d, Sr 4d states. Moreover, Fig. 7(a) clearly shows the change in the detailed structure of $\varepsilon_2(\omega)$, as we increase the Sr content; this results in the appearance of a new peak in the higher energy range as the composition x equals 0.50. This peak becomes more prominent when x equals 1.0, that is, for SrS.

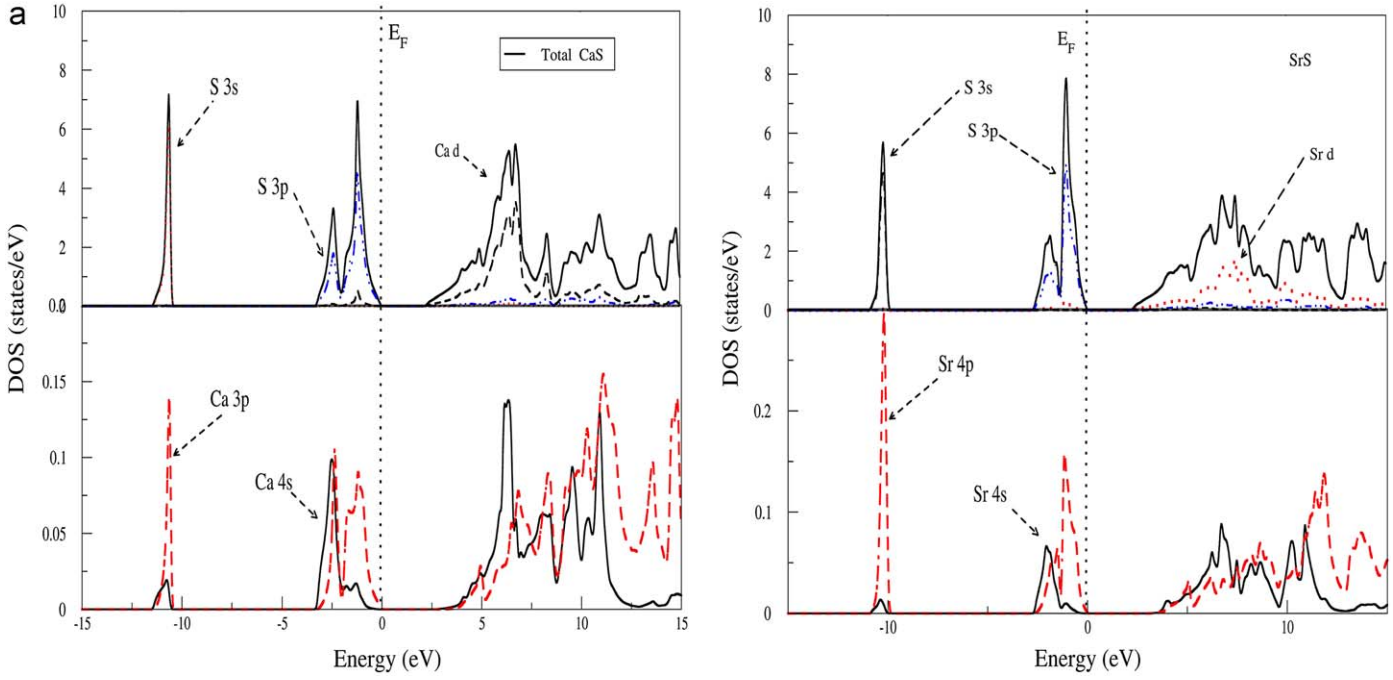

Fig. 6. (a) Partial density of states for CaS and SrS, (b) partial density of states for $Ca_{0.75}Sr_{0.25}S$, $Ca_{0.50}Sr_{0.50}S$ and $Ca_{0.25}Sr_{0.75}S$.

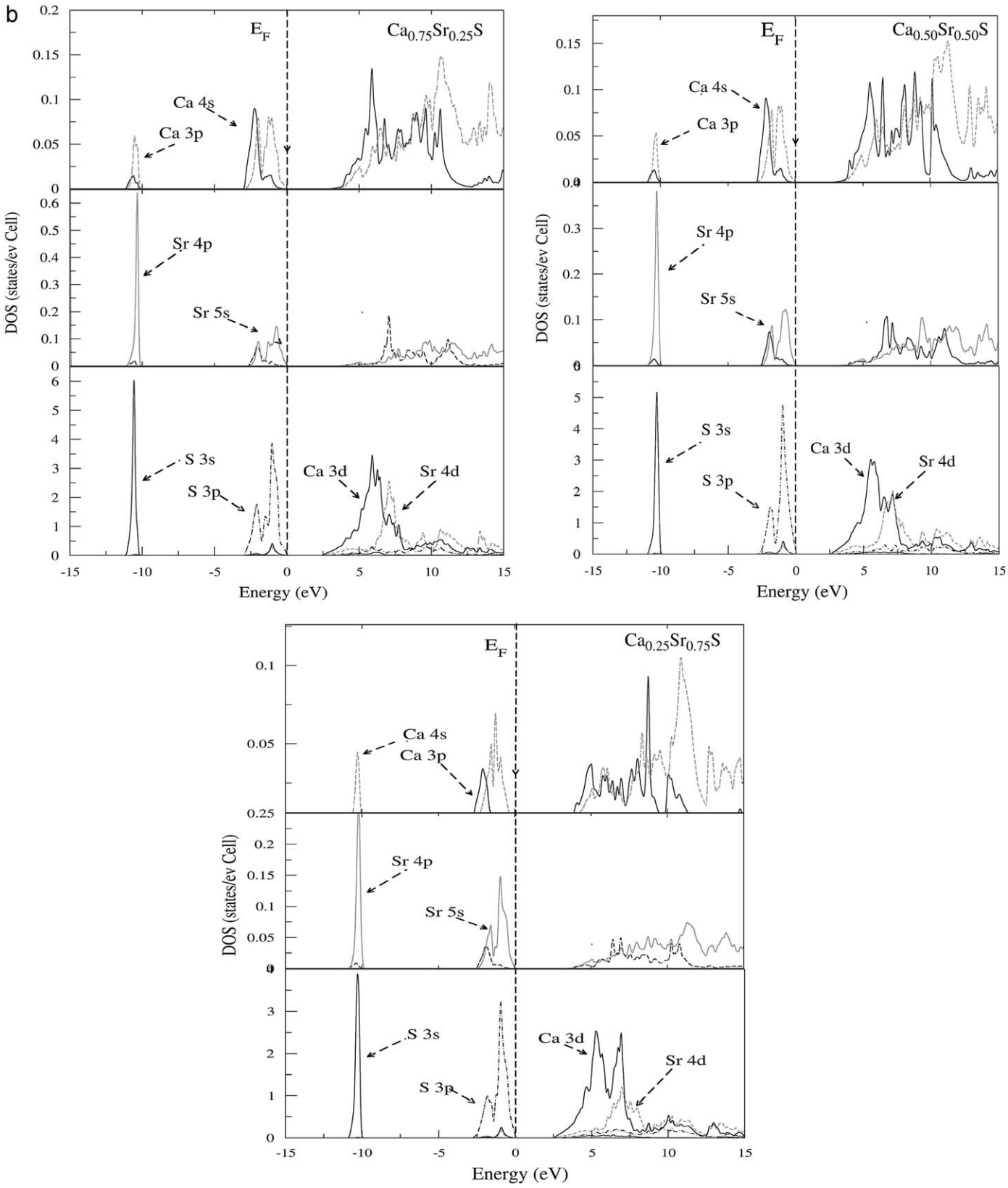

Fig. 6. (*Continued*)

Kaneko et al. [27] has measured the reflectivity spectra of alkaline-earth chalcogenides including CaS and SrS in the synchrotron radiation region of 4–40 eV. From observed reflectivity spectra, the spectra of the imaginary part of the dielectric constant, $\varepsilon_2(\omega)$, have been derived using the Kramers–Krönig transformation, and is shown in Fig. 4 of Ref. [27]. A careful comparison of our calculated spectra of $\varepsilon_2(\omega)$ with the experimentally determined spectra shows remarkable similarity in the

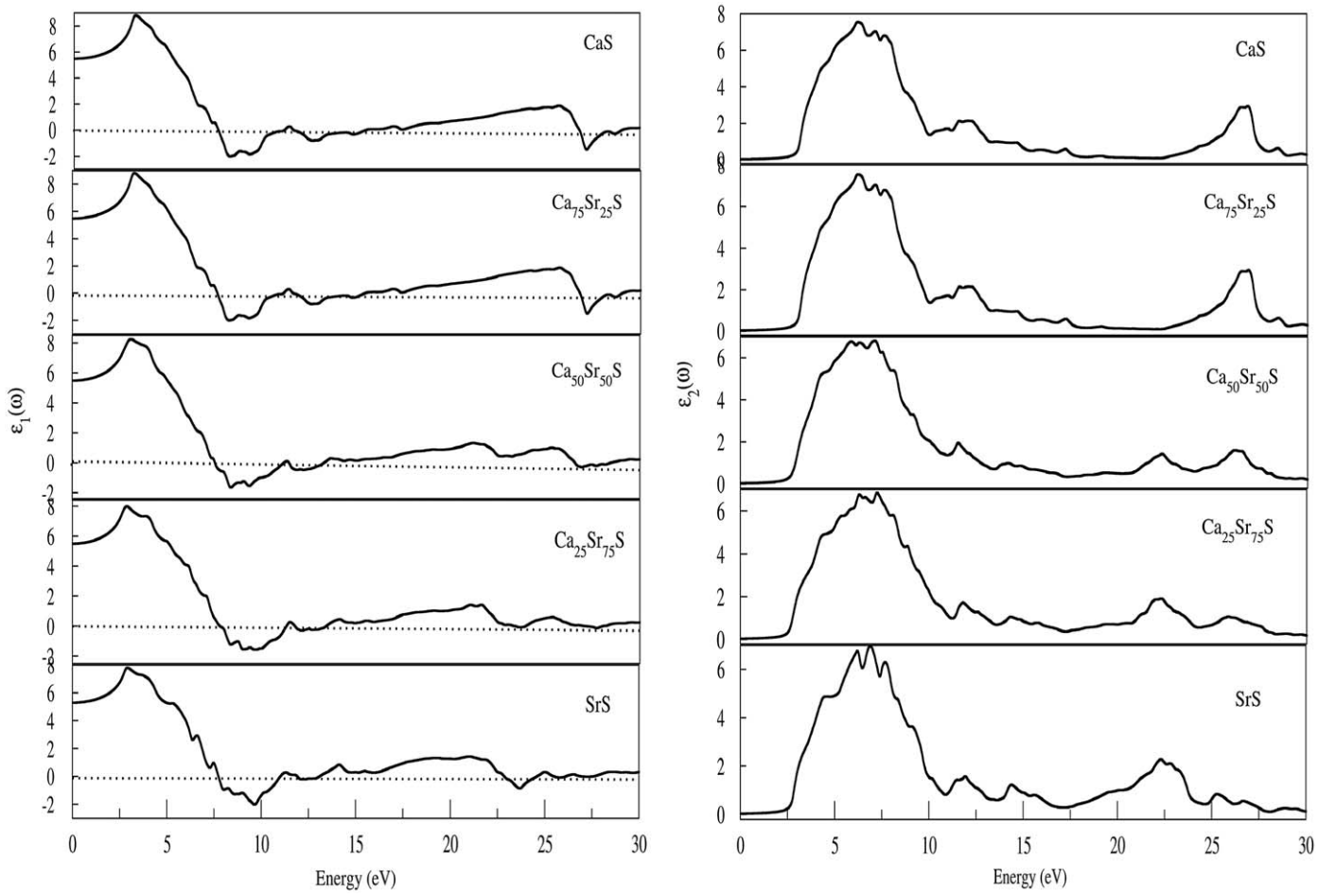

Fig. 7. Calculated real and imaginary parts of the dielectric function of $Ca_{1-x}Sr_xS$ corresponding to different value of x.

energy range of 4–20 eV for both CaS and SrS, although there are small differences in their detailed structure and a slight shift can be observed in the location of the strong peaks.

The real part of dielectric function, $\varepsilon_1(\omega)$, for $Ca_{1-x}Sr_xS$ alloys for the composition $x = 0.0$, 0.25, 0.50, 0.75 and 1.0 is displayed in Fig. 7(b). The main feature of the $\varepsilon_1(\omega)$ curves is: the occurrence of the strong peak in the energy range 2.4–5 eV for all compositions, then a rather steep decrease between 4.8 and 7.5 eV, after which it becomes negative, then a minimum followed by a slow increase at higher energies with a sharp decease around 26.8 eV for CaS. This feature changes significantly as we move towards SrS. The most important quantity of $\varepsilon_1(\omega)$ is the zero frequency limit $\varepsilon_1(0)$, which is the electronic part of static dielectric constant that strongly depends on the band gap. The calculated static dielectric constants for $Ca_{1-x}Sr_xS$ are 5.45, 5.45, 5.57, 5.40 and 5.28 for different concentration of x.

4. Conclusions

In this study, we have employed the FP-LAPW method within density functional theory in order to study the structural, electronic and optical properties of $Ca_{1-x}Sr_xS$ alloys. For the sake of comparison we have used all the three state-of-the-art approximations, namely the standard LDA, PBE GGA and the WC GGA. Calculated structural parameters clearly indicate that WC GGA results are closer to the experimental values as compared to those obtained by LDA and PBE GGA, whereas the results obtained for electronic properties (here band-gap values) are similar for all these approximations. For the compositional parameter value $x = 0.50$, we observe a structural phase transformation due to the charge transfer between the cation and anion. Electronic band structure and PDOS curves of the $Ca_{1-x}Sr_xS$ alloy system have been analyzed in terms of contribution from different orbitals of the constituent atoms. Furthermore, reasonable agreement is found between the calculated and experimental behavior of the imaginary part of the dielectric constant for the two end compounds CaS and SrS, while for their alloys no experimental data are available for comparison.

References

[1] R. Pandey, Mater. Sci. 5 (1986) 3357.
[2] S. Asano, N. Yamashita, Y. Nakao, Phys. Stat. Sol. 89 (1978) 663.
[3] Y. Nakanishi, T. Ito, Y. Hatanaka, G. Shimaoka, Appl. Surf. Sci. 66 (1992) 515.
[4] N. Yamashita, J. Phys. Soc. Japan 30 (1991) 3335.
[5] W. Lehmann, J. Electrochem. Soc. 117 (1970) 1389.
[6] T. Kato, H. Kagawa, H. Kanie, J. Crystal Growth 214/215 (2000) 958.
[7] J.W. Brightwell, B. Ray, P. Septhon, I.V.F. Viney, J. Crystal Growth 86 (1988) 634.
[8] C. Wang, K. Tang, Q. Yang, Y. Qian, J. Electrochem. Soc. 150 (2003) G163.
[9] P. Blaha, K. Schwarz, G.K.H. Madsen, D. Kvasnicka, J. Luitz, in: K. Schwarz (Ed.), WIEN2K, An Augmented Plane Wave+Local Orbitals Program for Calculating Crystal Properties, Techn. Universität, Wien, Austria, 2001, ISBN 3-9501031-1-2.
[10] J.P. Perdew, Y. Burke, M. Ernzerhof, Phy. Rev. Lett. 77 (1996) 3865.
[11] Z. Wu, R.E. Cohen, Phys. Rev. B 73 (2006) 235116.
[12] F.D. Murnaghan, Proc. Natl. Acad. Sci. USA 30 (1944) 244.
[13] H. Luo, R.G. Green, K. Ghandehari, T. Li, A.L. Ruoff, Phys. Rev. B 50 (1994) 16232.

[14] S. Ekbundity, A. Chizmeshya, R. LaViolette, G.H. Wolf, J. Phys. Condens. Matter 8 (1996) 8251.
[15] Z. Charifi, H. Baaziz, F. El Haj Hassan, N. Bouarissa, J. Phys. Condens. Matter 17 (2005) 4083.
[16] K. Syassen, Phys. Stat. Sol. (a) 91 (1985) 11.
[17] Y. Xiao-Cui, H. Ai-Min, Y. Jie, H. Yong-Hao, P. Gang, G. Chun-Xiao, Z. Guang-Tian, Chin. Phys. Lett. 25 (2008) 1807;
R. Khenata, H. Baltacheb, M. Rératc, M. Driza, M. Sahnounb, B. Bouhafsa, B. Abbarb, Physica B 339 (2003) 208.
[18] F. Tran, R. Laskowski, P. Blaha, K. Schwarz, Phys. Rev. B 75 (2007) 115131.
[19] L. Vegard, Z. Phys. 5 (1921) 17.
[20] Y. Kaneko, T. Koda, J. Crystal Growth 86 (1988) 72.
[21] Z.J. Chen, H.Y. Xiaa, X.T. Zua, Physica B 391 (2007) 193.
[22] S. Zhang, H. Li, H. Li, S. Zhou, X. Cao, J. Phys. Chem. B 111 (2007) 1304.
[23] V.S. Stepanyuk, A. Szász, O.V. Farberovich, A.A. Grigorenko, A.V. Kozlov, V.V. Mikhailin, Phys. Stat. Sol. (b) 155 (1989) 215.
[24] W.Y. Ching, F. Gan, M.Z. Huang, Phys. Rev. B 52 (1995) 1596.
[25] R. Pandey, J.E. Jaffe, A.B. Kunz, Phys. Rev. B 43 (1991) 9228.
[26] R.W. Godby, M. Schlüter, L.J. Sham, Phys. Rev. Lett. 56 (1986) 2415.
[27] M. Städele, J.A. Majevski, P. Vogel, A. Görling, Phys. Rev. Lett. 79 (1997) 2089.
[28] Y. Kaneko, K. Morimoto, T. Koda, J. Phys. Soc. Japan 52 (1983) 4385;
G.A. Saum, E.B. Hensley, Phys. Rev. 113 (1959) 1019.
[29] A.B. Kunz, Phys. Rev. B 26 (1982) 2056.
[30] D.M. Wood, A. Zunger, R. de Groot, Phys. Rev. B 33 (1985) 1026;
J.E. Bernard, A. Zunger, Phys. Rev. B 36 (1987) 3199.
[31] M.A. Khan, A. Kashyap, A.K. Solanki, T. Nautiyal, S. Auluck, Phys. Rev. B 48 (1993) 16974.